Eur. Phys. J. Special Topics **196**, 109–120 (2011)

DOI: 10.1140/epjst/e2011-01422-3

THE EUROPEAN PHYSICAL JOURNAL SPECIAL TOPICS

Review

X-ray scattering: Liquid metal/vapor interfaces

P.S. Pershan[a]

School of Engineering and Applied Sciences and the Physics Department Harvard University, Cambridge, MA, USA

Received 01 December 2010 / Received in final form 13 April 2011
Published online 30 May 2011

Abstract. We will review the principal x-ray scattering measurements that have been carried out on the free surface of liquid metals over the past two decades. For metals such as K, Ga, In Sn, Bi etc the surface induces well-defined layering with atomic spacing 'd' that penetrates into the bulk a distance of the order of the bulk liquid correlation length. As a consequence the angular dependence of the surface structure factor observed by x-ray reflectivity displays a broad peak at wavevector transfer $\sim 2\pi/d$ with a half width that is comparable to the width of the bulk liquid structure factor. Quantitative measurement of this surface structure factor requires correction for a singular Debye-Waller like effect arising from thermally excited capillary waves. For liquid metal alloys the layering is accompanied by chemical segregation (i.e. Gibbs absorption) that can be characterized from the energy dependence of the reflectivity. Particularly interesting are the temperature dependence and elasticity of the two-dimensional surface frozen phases that form on the surface of the $Au_{82}Si_{18}$ liquid eutectic. Surface freezing, although not observed near the eutectic points of alloys such as Au-Ge, Pd-Ge and Pd-Si, has been observed at the free surface of the glass forming alloy $Au_{49}Ag_{5.5}Pd_{2.3}Cu_{26.9}Si_{16.3}$.

1 Introduction

The objective of this paper is to provide a concise review of the principal structural properties that have been observed for various elemental liquid metals and alloys in the recent two to three decades since synchrotron measurements have become possible. These properties fall into two separate classes. The first corresponds to structure along the surface normal while the second is associated with structure parallel to the surface.

Of this first type the primary phenomena to be observed was the demonstration of atomic layering at the interface between the vapor and bulk. These first measurements for any liquid metal phases, that were accomplished for Hg and Ga in 1995, [1,2] occurred more than a decade after the effect was predicted by Rice and associates in the early 1980's [3,4]. The principal experimental issue that facilitated these measurements was the development in 1983 of an x-ray reflectometer capable of continuously deflecting a horizontal beam from a synchrotron downward by angles

[a] e-mail: Pershan@seas.harvard.edu

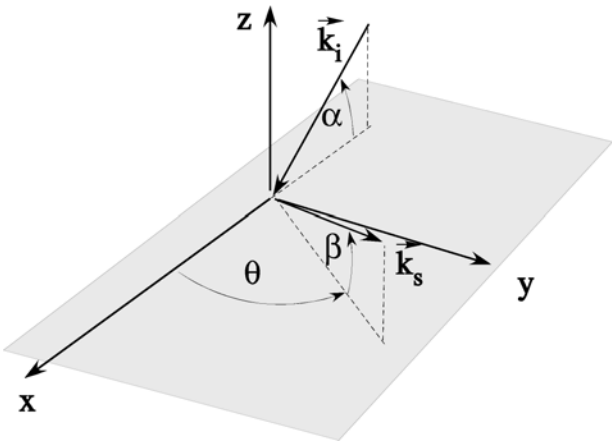

Fig. 1. Kinematics of x-ray reflectivity from a liquid surface. X-rays of wavevector $\vec{k}_i$ making an angle α to the surface are detected at an angle β at angle θ to the plane of incidence.

a that varied from zero to $\sim 10°$ to 15° [5,6]. The kinematics of x-ray scattering are illustrated in Fig. 1 for an x-ray wavevector, $\vec{k}_i$ incident at an angle α and detected at an angle β that can either be in the plane of incidence (i.e. $\theta = 0$) or at a finite angle.

The basic idea for the measurements starts with the idea that for an x-ray frequency ω that is large compared to the binding energy of the atomic electrons the index of refraction for the bulk liquid is well approximated by the free electron form

$$\varepsilon \approx 1 - 4\pi\rho_{bulk}e^2/m_e\omega^2 \tag{1}$$

where r_{bulk} is the effective electron density of the liquid, e and m_e are the electron charge and mass.[1] The angular frequency is $\omega = 2\pi c/\lambda$ and λ is the x-ray wavelength. For an abrupt flat interface between the vacuum and a material in which the electron density is everywhere equal to r_{bulk} the reflectivity for x-rays incident at an angle α is well approximated by the Fresnel form [7]

$$R_F(\alpha) = \left|\frac{\sin\alpha - \sqrt{\sin^2\alpha - \sin^2\alpha_c}}{\sin\alpha + \sqrt{\sin^2\alpha - \sin^2\alpha_c}}\right|^2 \underset{\alpha\gg\alpha_c}{\rightarrow} \left(\frac{\sin\alpha_c}{2\sin\alpha}\right)^4 \tag{2}$$

where $\sin^2\alpha_c \approx \alpha_c^2 = 4\pi\rho_{bulk}e^2/m_e\omega^2$. When the variation of the average electron density $\langle\rho(z)\rangle$ along the surface normal deviates from the abrupt step function, as occurs for example for a layered surface, the reflectivity is modified by an effective surface structure factor [7]

$$\Phi_{eff}(Q_z) \approx \rho_{bulk}^{-1}\int_{-\infty}^{+\infty} dz\,[\partial\langle\rho(z)\rangle/\partial z]\exp(iQ_z \bullet z) \tag{3}$$

to yield

$$R(Q_z) = R_F(Q_z)\,|\Phi_{eff}(Q_z)|^2 \tag{4}$$

[1] When the x-ray energy $\hbar\omega$ is large compared to the all of the electron binding energies r_{bulk} is the total electron density of the material. Otherwise it must be corrected to account for the dispersion of the atomic scattering factors.

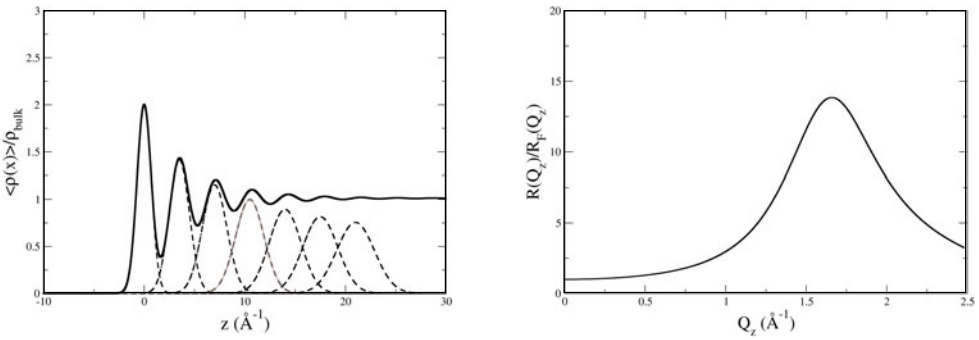

Fig. 2. (Left) Schematic illustration of the electron density profile associated with the distorted crystal model. (Right) The structure factor $|\Phi(Q_z)|^2$ that corresponds to the electron density to the left.

where $Q_z = (4\pi/\lambda)\sin\alpha$. For a surface in which $\rho_{bulk}^{-1}\left[\partial\left\langle\rho\left(z\right)\right\rangle/\partial z\right] = \delta\left(z\right)$ the surface structure factor $\Phi_{eff}\left(Q_z\right) = 1$ and $R\left(Q_z\right) = R_F\left(Q_z\right)$. The form of $\left\langle\rho\left(z\right)\right\rangle$ can be extracted from measurements of the dependence of $R\left(Q_z\right)$ on Q_z.

2 Surface induced atomic layering

One of the simplest illustrations of the effect of the surface structure factor on $R\left(Q_z\right)$ is the distorted crystal model (DCM) that is shown in the top panel of Fig. 2 [1]

$$\frac{\left\langle\rho\left(z\right)\right\rangle}{\rho_{bulk}} = \sum_{n=0}^{\infty}\frac{d}{\sigma_n\sqrt{2\pi}}\exp[-\left(z+nd\right)^2/\left(2\sigma_n^2\right)] \tag{5}$$

where d is the distance between atomic layers whose Gaussian widths are given by $\sigma^2 = \sigma_0^2 + n\bar{\sigma}^2$ with $n = (0, 1, 2, \ldots)$. The combination of the fact that the squared widths of the successive layers increase with distance from the surface along with the fact that the integrals of the densities have the same values for each of the layers leads to the constant density in the bulk material, far from the surface. Of the three parameters that enter this model the value of d determines the position, $Q_z^{peak} \approx 2\pi/d$, of the peak in $R(Q_z)/R_F(Q_z)$, the reciprocal of $\bar{\sigma}$ is proportional to the peak width, $\Delta Q_z^{peak} \sim 1/\bar{\sigma}$ and σ_0 fixes the peak amplitude. All three of these can be adjusted to produce functional forms for $R(Q_z)/R_F(Q_z) = |\Phi_{eff}(Q_z)|^2$ (Fig. 2, right) that agrees perfectly with measurements for Ga [2], In [8] and K [9]. Thus it was a surprise to discover that the structure factor $R(Q_z)/R_F(Q_z)$ for both liquid Sn [10] and Bi [11] have well defined *"bumps"* at values of Q_z well below Q_z^{peak} that are not predicted by the *DCM.*

3 Thermal capillary waves and the surface Debye-Waller effect

Before going any further it is important to appreciate the distinction between the effective structure factor that was introduced in Eq. (4) and the true, or local structure factor that describes the intrinsic surface induced atomic layering. Although the most commonly observed macroscopic liquid surfaces appear to be flat this is only because of gravity. On length scales that are less than $\sim$1 mm the principal force that opposes

thermal fluctuations $\langle|h(Q_{xy})|^2\rangle$ in the liquid height is surface tension, where $\vec{Q}_{xy}$ is a wavevector parallel to the surface [12,13]. According to the standard statistical physics so long as $Q_{Debye} > Q_{xy} \gtrsim mm^{-1}$ the mean square amplitude for the in-plane Fourier component of the fluctuations in the height of the liquid surface has the form [14–16]

$$\langle|h(Q_{xy})|^2\rangle \sim k_B T/\gamma Q_{xy}^2 \tag{6}$$

where g is the surface tension and $Q_{Debye} \sim 1/atomic\ size$. Height fluctuations at a finite value of Q_{xy} gives rise to diffuse scattering away from the specular condition. As illustrated in Fig. 1 for scattering at angles $\beta \neq \alpha$ and $\theta \neq 0$,

$$Q_{xy} \approx (2\pi/\lambda)\sqrt{\cos^2\alpha + \cos^2\beta - 2\cos\alpha\cos\beta\cos\theta}. \tag{7}$$

This scattering reduces the specular signal in the same way that phonons in solids give rise to a Debye-Waller factor that reduces the intensity of Bragg reflections in crystals.

One can show that in the region $Q_{Debye} > Q_{xy} \gtrsim mm^{-1}$ the differential cross section for scattering from a fluctuating liquid surface has the form [17]

$$\frac{d^2\sigma(\vec{Q})}{dQ_{xy}^2} \sim \left.\frac{d\sigma(\vec{Q})}{dQ_{xy}^2}\right|_F \left|\Phi(\vec{Q})\right|^2 \frac{1}{|Q_{xy}|^{2-\eta}} \tag{8}$$

where $d\sigma(\vec{Q})/dQ_{xy}^2|_F$ is the amplitude of the scattering cross-section for a flat, structure less surface and $\eta = (k_B T/2\pi\gamma)Q_z^2$. The function $|\Phi(Q_z)|^2 \neq |\Phi_{eff}(Q_z)|^2$ is the true *intrinsic* surface structure. The experimentally observed specular reflectivity is obtained by integration of $d^2\sigma(\vec{Q})/dQ_{xy}^2$ over the angular acceptance of the detector, $d^2\vec{Q}_{xy} = (2\pi/\lambda)^2 \sin\beta d\beta d\theta$. As an heuristic example note that if the detector resolution corresponded to a circle of radius ΔQ_{res} the integral of Eq. (8) would lead to a theoretical reflectivity of the form [8,18]

$$R(Q_z) = R_F(Q_z)\left|\Phi(Q_z)\right|^2 \left(\Delta Q_{res}/Q_{Debye}\right)^{\eta} = R_F(Q_z)\left|\Phi(Q_z)\right|^2 \exp\left[-2W_{DW}\right] \tag{9}$$

with a Debye-Waller factor

$$W_{DW} = Q_z^2 (k_B T/2\pi\gamma) \ln\left[Q_{Debye}/\Delta Q_{res}\right]. \tag{10}$$

Note that if $\Delta Q_{res} \to Q_{Debye}$ the Debye-Waller factor approaches zero and

$$R(Q_z) \to R_F(Q_z)\left|\Phi(Q_z)\right|^2.$$

On the other hand, in the more general case the intrinsic surface structure factor is larger than the effective surface structure in Eq. (4) by

$$\left|\Phi(Q_z)\right|^2 = \left|\Phi_{eff}(Q_z)\right|^2 \exp\left[+2W_{DW}\right] \tag{11}$$

where the actual values of $\exp[+2W_{DW}]$are best obtained by numerical integration of Eq. (8) over the experimental resolution [16].

The prototypical demonstration of this effect was the measurement of the temperature dependence of the reflectivity from the surface of liquid gallium. As shown by Regan et al. [19], (see Fig. 1 in [19]), although the peak value of $|\Phi_{eff}(Q_z)|^2$ decreases by a factor ~ 4 as the temperature increases from 22 °C to 160 °C, the

value of $|\Phi(Q_z)|^2$ that is obtained after division of $|\Phi_{eff}(Q_z)|^2$ by the calculated value of $\exp[+2W_{DW}]$ is constant, independent of temperature. In fact meaningful comparison between the reflectivities from different metals such as Ga, In and K with respective values of $T/g = [0.42, 0.77, 3.2]$ is only possible when the measured values of $R(Q_z)/R_F(Q_z) = |\Phi_{eff}(Q_z)|^2$ are divided by their respective calculated Debye-Waller term [9]. After division by the Debye-Waller factor the disparate reflectivities from these three metals are nearly identical [8,20]. Furthermore, unambiguous appraisal of the surprising low Q_z *bumps* that were referred to above for Sn[10] and Bi [11] with $T/g = [0.9, 1.43]$ are only clear when viewing $|\Phi(Q_z)|^2$ rather than $|\Phi_{eff}(Q_z)|^2$.

One of the unfortunate aspects of the experimental studies of liquid metal surfaces has been the lack of theoretical studies capable of quantitatively accounting for the reasons why some liquid metals follow the DCM and others do not. For example, even after more than two decades there is still not any explanation why the surface structure of liquid Hg as a very strong pronounced low Q_z dip that is not observed for any of the other elemental metals [1]. On the other hand there is reason to believe that this may now be changing. Most recently Calderin et al. carried out a first principles molecular dynamics simulation that predicted the observed low Q_z bump in the Sn structure factor [21].

In general the combination of the Debye-Waller factor, which scales as T/g and the necessity of maintaining atomically clean surfaces seriously constrains the elemental liquid metals that can be studied. With the exception of liquid Hg surface cleanliness requires UHV conditions which can not be achieved with liquids whose vapor pressure exceeds $\sim 10^{-6}$ torr at melting. With the exception of one or two more other elements, the relatively few systems mentioned above, Ga, In, K, Sn and Bi, are all that can be studied. On the other hand, there are a wealth of alloys with small values of T/g and low vapor pressure. In fact the surfaces of alloys introduce new physics beyond the surface induced layering that has been discussed so far.

4 Surface adsorption of binary alloys

Well over a century ago J. Willard Gibbs drew attention to the fact that the surface of a solution will be richer than the bulk in the element with the lower surface tension [22]. Although the argument is compelling it must eventually be balanced against a negative enthalpy of mixing that would favor the maximum coordination number between various elements in the mixture. It would thus seem that the surface structure of alloys should exhibit various combinations of surface induced atomic layering and surface adsorption.

One example of an alloy in which surface adsorption is the dominant effect is the binary Ga-Bi alloy whose phase diagram is illustrated in Fig. 3 [23–25]. The overall morphology of such a sample is shown in the central inset. It indicates a bulk thickness h of the lighter Ga-rich liquid on top of the heavier Bi-rich liquid. X-ray reflectivity measurements that were made along the lines DBMA revealed that the liquid/vapor interface was coated with a monolayer of Bi as expected from Gibbs, $g_{Bi} = 378\,\mathrm{erg/cm^2} < g_{Gq} = 718\,\mathrm{erg/cm^2}$. In addition to this Gibbs monolayer there is a macroscopic thickness, d, of the heavier Bi-rich liquid that wets the upper surface above the thickness h of the lighter Ga-rich liquid. X-ray reflectivity reveals that the thickness of this wetting layer increases along the segment D-B as the bulk phase approaches the coexistence line. This thickness remains essentially constant as the liquid is cooled from B-M along the coexistence line; however, on cooling below the monotectic point at 222 °C the sample assumes the morphology shown in the inset at the lower right where the bulk Ga-rich liquid coexists with the heavier solid Bi at

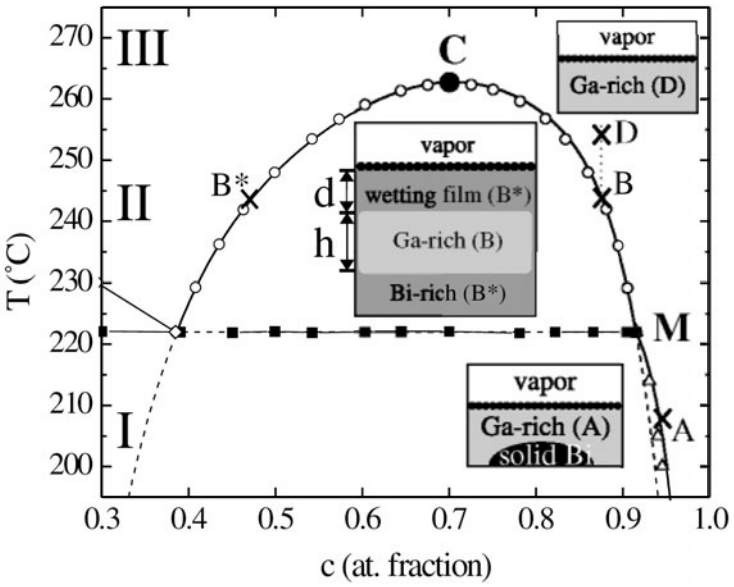

Fig. 3. Binary phase diagram for Ga-Bi. The open circles on the solid line indicated measured points on the miscibility gap between the Ga-rich and Bi-rich liquids. Point C is the consulate point. The horizontal line at $\sim 222\,^{\circ}\mathrm{C}$ indicates the monotectic point at which the two liquids are in thermal equilibrium with solid Bi. Below $222\,^{\circ}\mathrm{C}$ the bulk phase of the Ga-rich liquid is in thermal equilibrium with the bulk phase of solid Bi. The broken lines below $222\,^{\circ}\mathrm{C}$ indicate metastable extension of the miscibility gap of the liquid-liquid coexistence. The insets are discussed in the text.

the bottom. Along the line MA the Bi concentration in the Ga-rich liquid gradually decreases; however, x-ray reflectivity indicates that the surface remains coated with a finite thickness, d, of the metastable Bi rich liquid. The thickness of this metastable Bi-rich liquid gradually decreases on cooling from M to A for reasons analogous to the behavior between D and B. That is the line MA is off of the liquid-liquid coexistence curve, which is now a metastable coexistence line.

5 Surface frozen phases

The phase diagrams of Ga-Pb and Ga-Tl are topologically similar to that of Ga-Bi in that they all exhibit miscibility gaps along with a low temperature region in which the Ga-rich liquid coexists with either solid Pb, Tl or Bi. As is the case for the Ga-Bi system the surface tensions of Pb ($458\,\mathrm{erg/cm^2}$) and Tl ($464\,\mathrm{erg/cm^2}$) are less than that of Ga and, as was the case for Ga-Bi these surfaces were coated with monolayers of Pb and Tl. Yang et al. used a technique called *grazing incidence diffraction (GID)* to study the 2D order within the monolayer phases [26,27].

The idea behind GID can be understood from the expression for $R_{\mathrm{F}}(a)$ given by Eq. (2) when $\alpha < \alpha_c$ approaches grazing incidence [28,29]. In this limit $R_F\,(\alpha) = 1$ and there is 100% reflectivity, implying that the transmitted x-ray field is zero in the material below the surface. Of course this can't be completely true since the reflectivity is the result of an interaction between the incident field and the material but it does mean that the penetration into the material is limited to what is known as an *evanescent* region that is only tens of Ångstroms thick. For GID x-rays are incident at angles $\alpha < \alpha_c$ and detected at some angle θ away from the plane of incidence. If

both $\cos\alpha$ and $\cos\beta \approx 1$ the scattering vector parallel to the surface is of the order of $Q_{xy} \approx (4\pi/\lambda)\sin(\theta/2)$. Yang et al. observed the appearance of 2D Bragg scattering from either the Pb or Tl monolayer as the Ga-rich liquid were cooled to the liquidus line [26,27]. If surface induced atomic layering (i.e. Ga, In, K, Sn, Bi) is considered to be the first type of surface induced structure and the wetting layers and Gibbs absorption is the second type the appearance of 2D Bragg peaks, or surface freezing is yet a third type of surface induced order.

Surface frozen phases with long range 2-dimensional order have long been well known to form within thin Langmuir monolayers on water and other organic materials. More recently Deutsch and colleagues demonstrated similar phenomena when monolayers of organic molecules area deposited on the surface of liquid Hg [30–32]. In addition to this there are known examples of the appearance of long range 2D order due to surface freezing in neat organic liquids [33,34]. On the other hand, the only cases in which 2D surface freezing had been demonstrated for liquid metals appear to be when it is accompanied by some degree of surface adsorption, such as was discussed above for GaPb and GaTl. Below we will discuss a different case in which surface freezing for the $Au_{82}Si_{18}$ eutectic occurs well within the liquids region at temperature and concentrations that are not on the liquidus line [35,36].

On the other hand, before discussing the $Au_{82}Si_{18}$ eutectic it is worth noting that surface adsorption can be considerably richer than the simple Gibbs model. The prototypical example of this is the $Bi_{43}Sn_{57}$ eutectic [37]. The surface tension of Bi ($378\,\mathrm{erg/cm^2}$) is less than that of Sn ($560\,\mathrm{erg/cm^2}$) and according to Gibbs the surface should be rich in Bi. The experiments to probe the surface concentrations of this alloy made use of the fact that the form of the surface structure factor given by Eq. (3) is an approximation that ignores the dispersion in the atomic x-ray scattering amplitudes. X-ray reflectivity measurements for this alloy were taken at four different x-ray energies in the vicinity of the L3 absorption edge of Bi. The effective electron density that makes up the structure factor is a weighted average of the scattering from Bi and Sn; however, since the atomic scattering amplitude of Bi at the L3 edge is about 2/3 of its value away from the edge the effective electron density profile varies with energy in a way that reflects the distribution of Bi and Sn along the surface normal. The experiments revealed that although the first surface layer was $\sim$96 atm% Bi the second layer contained only $\sim$25 atm% Bi which is of the order of 60% of the bulk value while the third layer was again enriched in Bi over the bulk value. It is worth noting that the Sn-Bi surface pairing occurs in spite of the fact that the enthalpy of mixing for this alloy is rather small. Although these effects can be accounted for using lattice models such as those of either Defay-Prigogine [38] or Strohl-King [39] these are relatively crude and there is need for a more modern explanations.

To return to the surface freezing effect in the $Au_{82}Si_{18}$ eutectic alloy consider the effective structure factors shown in the top panel of Fig. 4 for T = 635 K (LT Phase), 695 K (HT Phase) and 720 K (LL Phase) [40]. The bottom panel illustrates the R/R_F at $Q_z = 1.4\,\text{Å}^{-1}$ that was measured on heating the sample at $\sim 5\,\mathrm{K/min}$. The sharp jumps between LT, HT and LL indicate reversible 1st order phase surface phase transitions. The most interesting thing about these plots is the fact that although the peak values of R/R_F for the HT and LL phases are comparable to the values observed for all other liquid metals the intensity for the LT phase is about an order of magnitude greater. The fact that GID revealed that the LT phase was a surface frozen phase with well developed long range 2D order originally led to an interpretation in which the large R/R_F was due to constructive interference between $\sim$6 to 7 very well developed surface layers [35]. As will be explained below, recent experiments clearly proved that this is not the case [40].

Aside from the intensity of the R/R_F there are two other important differences between the LT surface frozen phase of $Au_{82}Si_{18}$ and the surface frozen phases of the

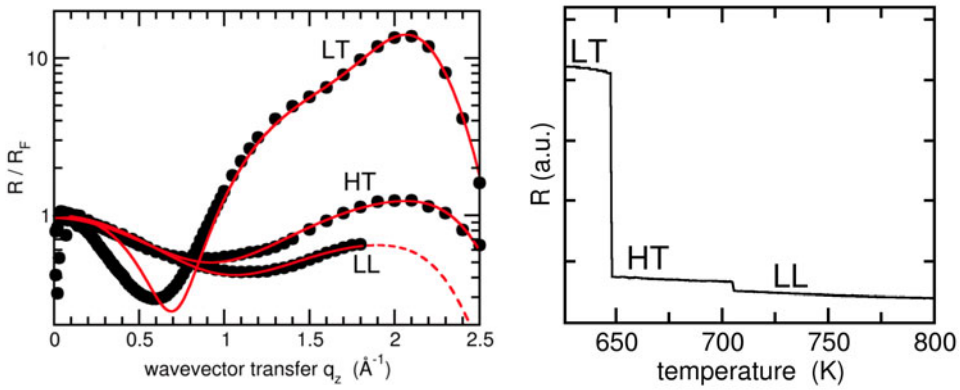

Fig. 4. (Right) Data for R/R_F measurements of the $Au_{82}Si_{18}$ eutectic alloy at T = 635 K (LT Phase), 695 K (HT Phase) and 720 K (LL Phase). The solid lines are best fits to model electron density profiles. (Left) Measurements of R/R_F vs. T at $Q_z = 1.4\,\text{Å}^{-1}$ [40].

GaPb and GaTl alloys. The first is that the LT phase exists for a range of ∼12 K that is well away from any phase boundary. Secondly, when the GID measurements are done by varying the detector angles, b and q, in order to measure the Bragg intensities as a function of Q_z for a fixed value of Q_{xy} (i.e. a truncation rod measurement) there is a well developed minimum at $Q_z \approx 0.95\,\text{Å}^{-1}$ that implies that the 2D surface frozen phase is an atomic bilayer with layer spacing of $d \approx \pi/0.95\,\text{Å} = 3.3\,\text{Å}$ [40]. Since it would be difficult to argue that there were ∼5 to 6 well developed surface layers when the GID shows only a bilayer there must be some other explanation for the large value of R/R_F. Before dealing with this; however, note that similar GID and truncation rod measurements show that at the LT to HT phase transition the bilayer LT surface frozen phase transforms into a monolayer with 2D long range order that is different from that of the LT. On further heating there is one more 1st order transition in which the surface frozen HT phase melts to form an ordinary liquid surface [40].

As we will now explain the large value of $R(Q_z)/R_F(Q_z) = |\Phi(Q_z)|^2 \exp[-2W_{DW}]$ in the LT occurs because the value of the Debye-Waller factor, W_{DW}, is reduced as a result of the elastic rigidity of the surface bilayer. The direct way by which this was confirmed was to measure diffuse scattering predicted by Eq. (8) as a function of q under grazing incidence conditions (i.e. h ≈ 0). Although the data for the LL phase follows the Q_{xy}^{-2} form of Eq. (8) out to values of $Q_{xy} \approx 0.25\,\text{Å}^{-1}$ the data for the LT phase has the faster fall off of $Q_{xy}^{-2}[1 + (Q_{xy}/Q_K)^2]^{-1}$ [14]. The value of the wavevector $Q_K \approx 0.1\,\text{Å}^{-1}$, which is a measure of the rigidity, is more than an order of magnitude smaller than the value of $1.16\,\text{Å}^{-1}$ which is the Debye wavevector for the LL eutectic surface. For the monolayer HT phase the value of $Q_K \approx 0.4\,\text{Å}^{-1}$. The solid lines through the $R(Q_z)/R_F(Q_z)$ data in Fig. 4 are best fits to the data using models for the intrinsic surface structure factors based on electron density profiles corresponding to a bilayer (LT), a monolayer (HT) and a simple DCM for the liquid (LL) phase.

As was mentioned above, one of the principle issues regarding the structure of liquid metal surfaces is the absence of theoretical explanations for the observed phenomena. This is especially clear for the $Au_{82}Si_{18}$ eutectic since there is no evidence for surface frozen phases for the relatively similar $Au_{72}Ge_{28}$ eutectic [41]. In fact experiments soon to be published have followed the surface scattering of ternary Au-Si-Ge

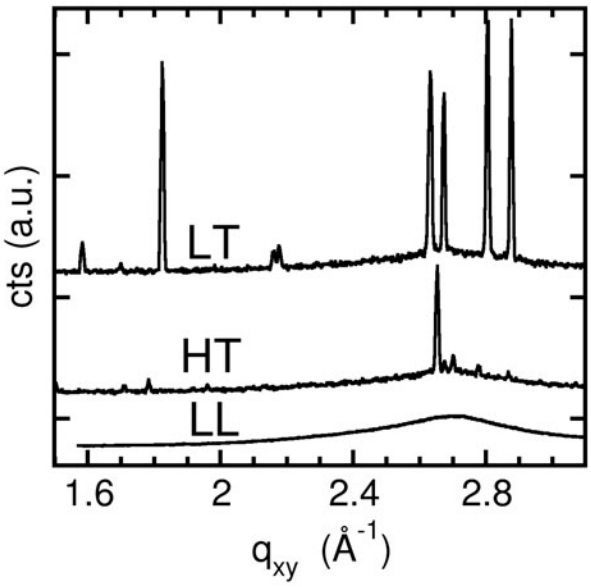

Fig. 5. Grazing incidence diffraction measurements from the $Au_{82}Si_{18}$ alloy at temperatures corresponding to the LT, HT and LL phases [40].

alloys for a number of concentrations along the eutectic line connecting these two binary eutectics [42]. Surface freezing is completely absent above ∼6.5 atm%Ge.

At the moment we do not have an explanation for the difference between the Au-Si and the Au-Ge alloys; however, a possible explanation might be associated with differences in the surface adsorption of Si and Ge. For example, resonant x-ray reflectivity measurements that were done on the Au-Ge alloy demonstrated that the surface concentration of Ge is essentially identical to the bulk value [41]. It isn't clear why this should be true since from the fact that the surface tensions of Ge, Si and Au are 621, 865 and 1169 erg/cm^2 respectively one might have expected a Gibbs monolayer of Ge. A similar measurement isn't possible for Si (lower Z). Nevertheless, the 2D Bragg peaks observed for the LT phase of $Au_{82}Si_{18}$ were well fit by a 2D unit cell with composition Au_4Si_8 that is considerably richer in Si than the bulk [35]. We don't have an explanation of why the surface should be richer in solute for Au-Si than for Au-Ge other than to speculate that it might be related to differences in the chemical pairing between Au-Si and Au-Ge. On the other hand, it isn't clear why the differences in surface concentrations would lead to different surface freezing even if the surface concentrations are different.

Another possibility is that the difference in surface freezing is related to the fact that the $Au_{82}Si_{18}$ system will form an amorphous metallic glass on rapid quenching, while $Au_{72}Ge_{28}$ does not [41]. In some way this might follow from differences in the short range order in the bulk phase of the two liquids. Unfortunately, this can't be the entire explanation since surface frozen phases were not observed for the good glass forming Pd-Si and Pd-Ge alloys which do possess significant degrees of short range order [43]. On the other hand, lest one think that the $Au_{82}Si_{18}$ is unique our most recent experiment found a surface frozen phase for the glass forming alloy $Au_{49}Ag_{5.5}Pd_{2.3}Cu_{26.9}Si_{16.3}$ [44,45].

Finally, there is one other soon to be published result on the surface structure of the $Pd_{81}Ge_{19}$ alloy [43]. Although this system did not exhibit surface freezing of the type discussed above the x-ray reflectivity did contain a series of oscillations at

very low values of Q_z with a period $\Delta Q_z \approx 2\pi/40$ Å^{-1} that are completely unlike anything that was observed in any other liquid metal. The only possible explanation for this anomaly is the existence of an ∼40 Å thick surface layer with an electron density that is ∼4% larger than that of the bulk material. The most likely rationale for this is the accumulation at the surface of the kinds of ∼40 Å clusters that are known to form in many other metallic alloys [46].

6 Summary

The intent of this article has been to provide a brief synopsis of the x-ray studies of the surfaces of metals that have been done by both our group and others and to also show some avenues for future work. The first experiments that were done concentrated on the surface induced atomic layering along the normal to the liquid/vapor interface. With time it became obvious that in order to obtain a true measure of the intrinsic structure it was necessary to correct the measured data for the rather severe Debye-Waller effects due to thermally induced capillary fluctuations in the height of the surface. In most cases this is straightforward; however, as we eventually demonstrated surface frozen 2D in-plane order gives rise to elastic rigidity that can have a profound effect on the Debye-Waller factor. This became clear for interpretation of the reflectivity from the LT surface frozen phase of the $Au_{82}Si_{18}$ eutectic liquid.

Other phenomena that were discussed included the use of resonant x-ray scattering to probe atomic demixing at the surface of the Sn-Bi alloy, wetting of the surface of the binary Ga-Bi phase along with surface freezing of the Gibbs monolayers of Pb and Tl at the surface of Ga alloys. Although surface freezing at solid /liquid coexistence, as for the Ga alloys of Pb and Tl seems straightforward the explanation for why there surface freezing of the $Au_{82}Si_{18}$ eutectic away from coexistence, and why it does not occur for $Au_{72}Ge_{28}$ and the Pd alloys of Si and Ge is not explained. On the other hand, the discovery of surface freezing for the $Au_{49}Ag_{5.5}Pd_{2.3}Cu_{26.9}Si_{16.3}$ demonstrates that these phenomena need to be more widely explored. Finally, for many of these experiments there is a compelling need for quantitative theoretical explanations.

Those experimental results discussed here that were done by the Harvard group involved over two dozen collaborators over roughly two decades. Although it is not practical to individually acknowledge each of them their names appear as coauthors on the various literature citations below. Nevertheless, especial acknowledgment is due to Stefan Mechler for the most recent work that was only possible through his efforts. Similarly, I would like to acknowledge the two decades of support from the U.S. Department of Energy, Office of Basic Energy Sciences, Division of Materials Sciences and Engineering under Award DE-FG02-88ER45379.

References

1. O.M. Magnussen, B.M. Ocko, M.J. Regan, K. Penanen, P.S. Pershan, M. Deutsch, Phys. Rev. Lett. **74**, 4444 (1995)
2. M.J. Regan, E.H. Kawamoto, S. Lee, P.S. Pershan, N. Maskil, M. Deutsch, O.M. Magnussen, B.M. Ocko, L.E. Berman, Phys. Rev. Lett. **75**, 2498 (1995)
3. M.P. Develyn, S.A. Rice, J. Chem. Phys. **78**, 5225 (1983)
4. S.A. Rice, Proc. Natl. Acad. Sci. USA **84**, 4709 (1987)
5. J. Als-Nielsen, P.S. Pershan, Nuclear Inst. Methods **208**, 545 (1983)
6. P.S. Pershan, J. Als-Nielsen, Phys. Rev. Lett. **52** 759 (1984)
7. P.S. Pershan, A. Braslau, A.H. Weiss, J. Als-Nielsen, Phys. Rev. A **35**, 4800 (1987)

8. H. Tostmann, E. DiMasi, P.S. Pershan, B.M. Ocko, O.G. Shpyrko, M. Deutsch, Phys. Rev. B **59**, 783 (1999)
9. O.G. Shpyrko, M. Fukuto, P.S. Pershan, B.M. Ocko, T. Gog, I. Kuzmenko, M. Deutsch, Phys. Rev. B **69**, 245423 (2004)
10. O.G. Shpyrko, A. Grigoriev, C. Steimer, P.S. Pershan, B. Lin, M. Meron, T. Graber, J. Gerbhardt, B.M. Ocko, M. Deutsch, Phys. Rev. B **70**, 224206 (2004)
11. P.S. Pershan, S. Stoltz, O. Shpyrko, M. Deutsch, V. Balagurusamy, M. Meron, B. Lin, R. Streitel Phys. Rev. B **79**, 115417 (2009)
12. R. Lovett, C.Y. Mou, F.P. Buff, J. Chem. Phys. **65**, 570 (1976)
13. P.S. Pershan, Colloids & Surfaces A **171**, 149 (2000)
14. J. Daillant, L. Bosio, J. Benattar, J. Meunier, Europhys. Lett. **8**, 453 (1989)
15. A. Braslau, M. Deutsch, P.S. Pershan, A.H. Weiss, J. Als-Nielsen, J. Bohr, Phys. Rev. Lett. **54** 114 (1985)
16. A. Braslau, P. Pershan, G. Swislow, B. Ocko, N.J. Als, Phys. Rev. A **38**, 2457 (1988)
17. S.K. Sinha, E.B. Sirota, S. Garoff, H.B. Stanley, Phys. Rev. B **38**, 2297 (1988)
18. P.S. Pershan, J. Phys. Chem. B **113**, 3639 (2009)
19. M. Regan, P. Pershan, O. Magnussen, B. Ocko, M. Deutsch, L. Berman, Phys. Rev. B **54**, 9730 (1996)
20. O.G. Shpyrko, P. Huber, P.S. Pershan, B.M. Ocko, H. Tostmann, A. Grigoriev, M. Deutsch, Phys. Rev. B **67**, 115405 (2003)
21. L. Calderín, L.E. González, D.J. González, Phys. Rev. B **80**, 115403 (2009)
22. J.W. Gibbs, R.G. Van Name, W.R. Longley, H.A. Bumstead, *The collected works of J. Willard Gibbs* (New York, Longmans, Green and Co., 1928)
23. D. Nattland, P.D. Poh, S.C. Müller, W. Freyland, J. Phys.: Cond. Matt. **7**, L457 (1995)
24. P. Huber, O. Shpyrko, P.S. Pershan, B. Ocko, E. DiMasi, M. Deutsch, Phys. Rev. B **68**, 085401 (2003)
25. P. Huber, O. Shpyrko, P.S. Pershan, B.M. Ocko, H. Tostmann, E. DiMasi, M. Deutsch, Phys. Rev. Lett. **89**, 035502 (2002)
26. B. Yang, D. Gidalevitz, D. Li, Z. Huang, S.A. Rice, Proc. Natl. Acad. Sci. USA **96**, 13009 (1999)
27. B. Yang, D.X. Li, S.A. Rice, Phys. Rev. B **67**, 212103 (2003)
28. W.C. Marra, P.E. Eisenberger, A.Y. Cho, J. Appl. Phys. **50**, 6927 (1979)
29. S. Dietrich, H. Wagner, Z. Phys. B **56**, 207 (1984)
30. H. Kraack, B.M. Ocko, P.S. Pershan, E. Sloutskin, M. Deutsch, Science **298**, 1404 (2002)
31. H. Kraack, L. Tamam, E. Sloutskin, M. Deutsch, B.M. Ocko, Langmuir **23**, 7571 (2007)
32. L. Tamam, H. Kraack, E. Sloutskin, B.M. Ocko, P.S. Pershan, M. Deutsch, Thin Sol. Films **515**, 5631 (2007)
33. X.Z. Wu, E.B. Sirota, S.K. Sinha, B.M. Ocko, M. Deutsch, Phys. Rev. Lett. **70**, 958 (1993)
34. M. Deutsch, X.Z. Wu, E.B. Sirota, S.K. Sinha, B. Ocko, O. Magnussen, Europhys. Lett. **30**, 283 (1994)
35. O.G. Shpyrko, R. Streitel, V.S.K. Balagurusamy, A.Y. Grigoriev, M. Deutsch, B.M. Ocko, M. Meron, B.H. Lin, P.S. Pershan, Science **313**, 77 (2006)
36. O.G. Shpyrko, R. Streitel, V.S.K. Balagurusamy, A.Y. Grigoriev, M. Deutsch, B.M. Ocko, M. Meron, B. Lin, P.S. Pershan, Phys. Rev. B **76**, 245436 (2007)
37. O.G. Shpyrko, A.Y. Grigoriev, R. Streitel, D. Pontoni, P.S. Pershan, M. Deutsch, B.M. Ocko, Phys. Rev. Lett. **95**, 106103 (2005)
38. R. Defay, I. Prigogine, A. Bellemans, *Surface tension and adsorption* (New York, Wiley, 1966)
39. J.K. Strohl, T.S. King, J. Catal. **118**, 53 (1989)
40. S. Mechler, P.S. Pershan, S. Stoltz, E. Yahel, O. Shpyrko, B. Lin, M. Meron, S. Sellner, Phys. Rev. Lett. **105**, 186101 (2010)
41. P.S. Pershan, S.E. Stoltz, S. Mechler, O.G. Shpyrko, A.Y. Grigoriev, V.S.K. Balagurusamy, Phys. Rev. B **80**, 125414 (2009)

42. S. Mechler, S. Sellner, V.S.K. Balagurusamy, S.E. Stoltz, P.S. Pershan, E. Yahel, O. Shpykro, M. Meron, B. Lin (in preparation) (2010)
43. S. Mechler, E. Yahel, P.S. Pershan, S.E. Stoltz, B. Lin, M. Meron (in preparation) (2010)
44. T.W. Tang, Y.C. Chang, J.C. Huang, Q. Gao, J.S.C. Jang, C.Y.A. Tsao, Mater. Chem. Phys. **116**, 569 (2009)
45. S. Mechler, E. Yahel, P.S. Pershan, S.E. Stoltz, B. Lin, M. Meron (in preparation) (2010)
46. K. Urban, M. Feuerbacher, J. Non-Cryst. Sol. **334-335**, 143 (2004)